

Optical Oxygen Sensing Material: Terbium(Ⅲ) Complex Adsorbed Thin Film

Yutaka Amao,* Yuichi Ishikawa, Ichiro Okura,† and Tokuji Miyashita††

Department of Applied Chemistry, Oita University, Dannoharu, Oita 870-1192

†Department of Bioengineering, Tokyo Institute of Technology, Nagatsuta, Midori-ku, Yokohama 226-8501

††Institute of Multidisciplinary Research for Advanced Materials, Tohoku University, Katahira, Aoba-ku, Sendai 980-8577

(Received May 18, 2001)

A new optical oxygen sensor based on the luminescence intensity change of a terbium(Ⅲ) complex, tris(acethylacetonato)(1,10-phenanthroline)terbium(Ⅲ) complex, ([Tb(acac)$_3$(phen)]), adsorbed thin film onto an alumina plate, was developed. The luminescence peak positions of [Tb(acac)$_3$(phen)] film were observed at 490, 546, 590 and 620 nm. The luminescence intensities of [Tb(acac)$_3$(phen)] in the film decreased with increasing the oxygen concentration, indicating that the film can be used as an optical oxygen sensing device based on luminescence quenching by oxygen. The ratio I_0/I_{100} (I_0 and I_{100} represent the detected luminescence intensities from the film exposed to 100% argon and 100% oxygen, respectively) values of [Tb(acac)$_3$(phen)] film are estimated to be 2.66 (490 nm), 2.68 (546 nm), 2.67 (590 nm) and 2.66 (620 nm), respectively. [Tb(acac)$_3$(phen)] film obeyed a Stern–Volmer plot with a multi-site model and possessed good operational stability. The response times of the [Tb(acac)$_3$(phen)] film were 7.3 s for switching from argon to oxygen, and 70 s for switching from oxygen to argon.

Determining the oxygen concentration is important in various fields of chemical, clinical analysis and environmental monitoring.[1–3] Several oxygen detection systems have been reported i.e., some based on titration[4] as well as amperometric,[5] chemiluminescence,[6] or thermoluminescence determinattions.[7] The most successful method has been the oxygen-electrode method. However, it is limited by the stability of the electrode surface and by instabilities in the oxygen diffusion barrier, because it measures the rate of diffusion of oxygen to the cathode. A number of luminophores has been used as oxygen-sensing probes for optical oxygen sensors.[8–10] Many optical oxygen sensors are composed of organic dyes, such as polycyclic aromatic hydrocarbons (pyrene and its derivatives, quinoline and phenanthrene) immobilized in an oxygen permeable polymer.[11,12] Polycyclic aromatic hydrocarbons have a strong fluorescence with long fluorescence lifetimes like 200 ns, which make them very amenable to quenching by oxygen. Recently, much attention has been given to the photochemical and photophysical properties of lanthanide complexes.[13–22] Terbium(Ⅲ) complexes display remarkably strong green luminescence with a high quantum yield, and have a long lifetime.[22] The luminescence processes of the terbium(Ⅲ) complexes are as follows. The intersystem crossing process form the photoexcited singlet state of the ligand to the photoexcited triplet state of the ligand occurs, and then energy transfer from the photoexcited triplet state of the ligand to the excited state of terbium(Ⅲ) ion (the energy level of $^5D_4$) takes place. The luminescence of the terbium(Ⅲ) complexes is attributed to the 4*f* orbital–4*f* orbital transition (the energy level of excited state $^5D_4$ to the energy level of the ground state ^7F_j).[17–22] The green luminescence is attributed to the $^5D_4$ to ^7F_j transition. Thus, the terbium(Ⅲ) complexes are attractive candidates as novel optical oxygen-sensing materials. In general, the oxygen-sensing dye molecules immobilized in organic polymer films have usually been used for an optical oxygen sensor. Because dye molecules were found to interact with polymer molecules directly, the properties of sensing films strongly depend on the properties of the polymer. To overcome these problems, a dye adsorption film has been exploited. Especially, the dye molecules were strongly adsorbed onto alumina surface. Because the sensing dyes can be immobilized on the alumina surface directly by using this technique, a highly sensitive device for oxygen sensing will be accomplished by using a dye adsorption film.

In this work, terbium(Ⅲ) complexes, tris(acethylacetonato)(1,10-phenanthroline)terbium(Ⅲ) complex, ([Tb(acac)$_3$(phen)]), (the chemical structure is shown in Fig. 1) was ap-

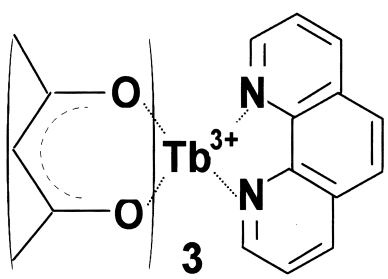

[Tb(acac)$_3$(phen)]

Fig. 1. Chemical structure of [Tb(acac)$_3$(phen)].

plied to an optical oxygen sensing probe, and the oxygen-sensing properties of [Tb(acac)$_3$(phen)] adsorbed film onto alumina plate were studied.

Experimental

[Tb(acac)$_3$(phen)] was prepared by adding 40 mL of a warm ethanolic solution of 1,10-phenanthroline (1 mmol) to an ethanolic solution containing 1 mmol of tris(acethylacetonato)terbium(III) (obtained from Aldrich) at 70 °C for 5 h. [Tb(acac)$_3$(phen)] was characterized by the UV-vis absorption spectrum. During the synthesis of [Tb(acac)$_3$(phen)], the intensity of the absorption band at 268.1 nm attributed to the coordination of 1,10-phenanthroline, increased. The precipitate was filtered, washed with ethanol and dried in a vacuum. Purification was performed by recrystallization from an ethanol–water (1:2) mixture. A [Tb(acac)$_3$(phen)] adsorbed thin film was prepared as follows. An alumina plate was dipped into 0.1 mmol dm^{-3} [Tb(acac)$_3$(phen)] in a dichloromethane solution at room temperature for 30 min. After dipping, the plate was washed with water and ethanol several times. The films were dried at room temperature and stored in the dark prior to use. An alumina plate was prepared by anodic oxidation of the aluminium plate. The aluminium plate (1.2 × 4 cm) was washed with a NaOH aqueous solution for 2 min, and was then electrically oxidized in a 1.0 mol dm^{-3} H_2SO_4 solution for 30 min. After oxidation, the plate was washed with a H_3PO_4 solution for 10 min. The alumina plates were dried in a vacuum at 80 °C for 5 h and stored in the vacuum prior to use.

The UV-vis absorption spectrum of the [Tb(acac)$_3$(phen)] in dichloromethane solution was recorded using a Shimadzu UV-2400PC spectrometer. Steady state luminescence spectra and the excitation spectra of the [Tb(acac)$_3$(phen)] film were measured using a Shimadzu RF-5300PC Spectrofluorophotometer with a 150 W xenon lamp as a visible excitation light source. The excitation and emission bandpasses were 5.0 nm.

Oxygen sensing was carried out using a spectrofluorophotometer with a 150 W Xenon lamp as the excitation light source. The sample film was mounted at a 45° angle in the quartz cell to minimize any light scattering from the sample and substrate. Different oxygen standards (in the range 0–100%) in a gas stream were produced by controlling the flow rates of oxygen and argon gases entering a mixing chamber. The total pressure was maintained at 760 Torr (1 Torr = 133.322 Pa).[23] All of the experiments were carried out at room temperature. The oxygen-sensing properties of [Tb(acac)$_3$(phen)] film were characterized by the Stern-Volmer quenching constant (K_{SV}) obtained from the following equation (1):

$$(I_0/I) - 1 = K_{SV}\,[O_2], \quad (1)$$

where I_0, I and [O_2] are the luminescence intensities in the absence and presence of oxygen and the oxygen concentration, respectively. The K_{SV} value was obtained from a linear plot of $(I_0/I) - 1$ versus [O_2].

Results and Discussion

The reflectance spectrum of the [Tb(acac)$_3$(phen)] film is shown in Fig. 2. The shape of the spectrum of the [Tb(acac)$_3$(phen)] film was almost the same as that in a dichloromethane solution (absorption peak position = 268.3 and 228.2 nm for film and 268.1 and 228.1 nm in dichloromethane solution), and no peak shift was observed. Thus, [Tb(acac)$_3$(phen)] was homogeneously adsorbed to the alumina plate.

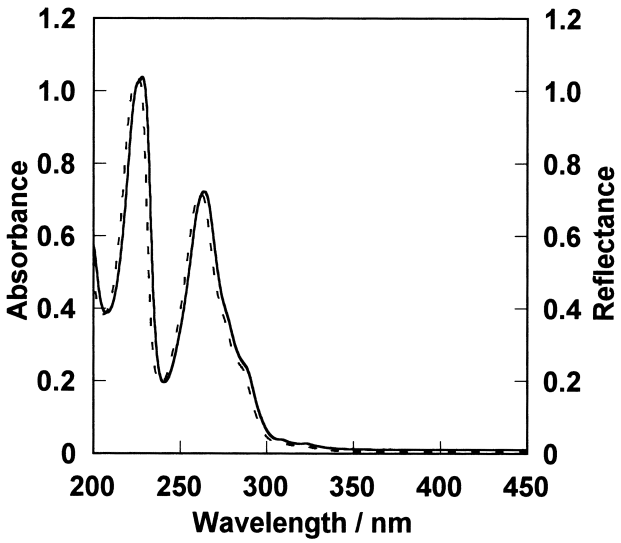

Fig. 2. The reflectance spectra of [Tb(acac)$_3$(phen)] film (solid line). The UV-vis absorption spectra of [Tb(acac)$_3$(phen)] in dichloromethane solution (dash line).

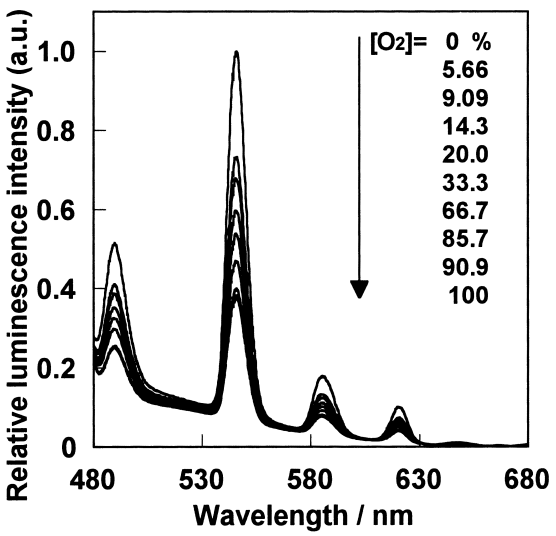

Fig. 3. The luminescence spectra of [Tb(acac)$_3$(phen)] film under various oxygen concentrations. Excitation wavelength was 268 nm.

The luminescence spectra of the [Tb(acac)$_3$(phen)] film under various oxygen concentrations are shown in Fig. 3. The luminescence peak positions of the film were observed at 490 (attributed to $^5D_4$ to $^7F_1$ transition), 546 (attributed to $^5D_4$ to $^7F_2$ transition), 590 (attributed to $^5D_4$ to $^7F_3$ transition) and 620 nm (attributed to $^5D_4$ to $^7F_4$ transition). The excitation wavelength was 268 nm, and is attributed to the 1,10-phenanthroline ligand. The intensities of the luminescence peak positions of the [Tb(acac)$_3$(phen)] film depended on the oxygen concentration. The intensities of the [Tb(acac)$_3$(phen)] film at 490, 546, 590 and 620 nm decreased with increasing the oxygen concentration, as shown in Fig. 4. In this figure, the reference is the luminescence intensity at 546 nm under 100% argon conditions. The ratio I_0/I_{100} is used as a measure of the film sensitiv-

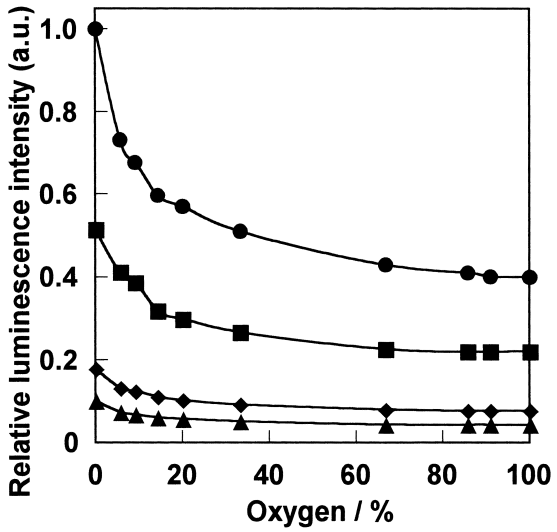

Fig. 4. The relative luminescence intensity changes of [Tb(acac)$_3$(phen)] film under various oxygen concentrations. Emission wavelength: (■) 490, (●) 546, (◆) 590 and (▲) 620 nm.

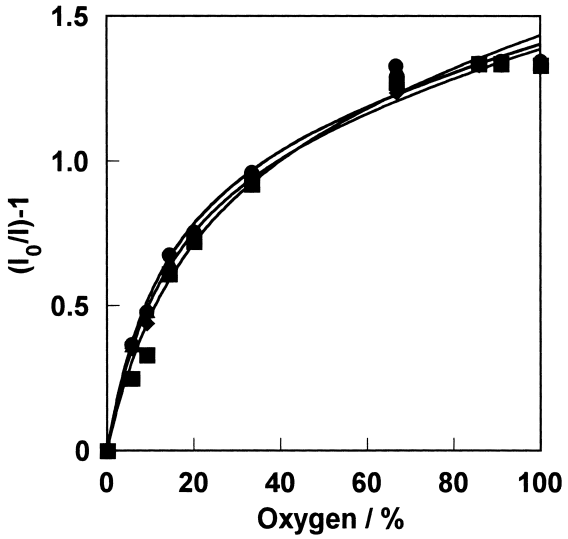

Fig. 5. Stern–Volmer plot for [Tb(acac)$_3$(phen)] film. Emission wavelength: (■) 490, (●) 546, (◆) 590 and (▲) 620 nm

ity, where I_0 and I_{100} represent the detected luminescence intensities from the film exposed to 100% argon and 100% oxygen, respectively. The I_0/I_{100} values of the [Tb(acac)$_3$(phen)] film are estimated to be 2.66 (490 nm), 2.68 (546 nm), 2.67 (590 nm) and 2.66 (620 nm), respectively. For all of the monitored wavelengths, the I_0/I_{100} values were almost the same. This result indicates that the luminescence of [Tb(acac)$_3$(phen)] in the film is quenched by oxygen, and that this film can thus be used as an optical oxygen sensing device by employing its oxygen-induced luminescence quenching ability as an indicator of the oxygen concentration.

Figure 5 shows Stern–Volmer plots for the [Tb(acac)$_3$(phen)] film monitored at 490, 546, 590 and 620 nm. For all cases, the plots exhibit considerable linearity at lower oxygen concentrations, although the curvature decreases at higher oxygen concentrations. Usually, the results of downward curvature in Stern–Volmer plots at higher oxygen concentrations have been explained by two different theories: one being the coexistence of dynamic and static quenching processes, and the other by the fact that dynamic quenching is the sole quenching process in an optical oxygen sensor system with differences in sites occupied by dye molecules with different oxygen accessibility. The simultaneous presence of dynamic and static quenching when the luminescence of [Tb(acac)$_3$(phen)] is quenched both by excited state collisions, ([Tb(acac)$_3$(phen)]---O_2)* and by ground-state complex formation with the oxygen, [Tb(acac)$_3$(phen)]---O_2,as shown in Scheme 1.

In the scheme, [Tb(acac)$_3$(phen)]* is the photoexcited state of [Tb(acac)$_3$(phen)] and k_r, k_d, k_{-d} and k_{nr} are the rate constants for the radiative decay, diffusion, back diffusion and non-radiative quenching, respectively. The relative luminescence intensity (I_0/I) is given by the product of both the dynamic and static quenching.[25] Hence,

$$I_0/I = (1 + K_D[O_2])(1 + K_S[O_2]) = 1 + K_1[O_2] + K_2[O_2]^2, \quad (2)$$

$$I_0/I = (1 + K_D[O_2]) \exp(K_T[O_2]), \quad (3)$$

$$K_T = (N_a V/1000)[4\pi R^2 (D\tau)^{1/2}], \quad (4)$$

where, K_D and K_S are the dynamic and static quenching constants, respectively, and $K_1 = K_D + K_S$ and $K_2 = K_D K_S$. If there is a transient component present in dynamic quenching,[25] then K_T is the transient quenching constant, N_a is Avogadro's number and V and R are the volume and radius of the transient quenching sphere; D and T are the viscosity of the medium and the lifetime of the [Tb(acac)$_3$phen], respectively. For weak quenching,

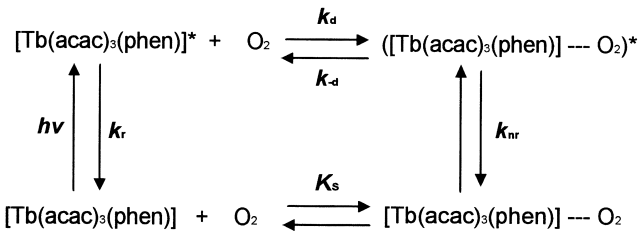

Scheme 1. Quenching processes of [Tb(acac)$_3$(phen)] by oxygen. The luminescence of [Tb(acac)$_3$(phen)] can be quenched not only through excited state collision ([Tb(acac)$_3$(phen)]---O_2)* but also through ground state collision [Tb(acac)$_3$(phen)]---O_2.

$$I_0/I = (1 + K_D[O_2])(1 + K_T[O_2]) = 1 + K_1[O_2] + K_2[O_2]^2. \quad (5)$$

Thus, the overall dynamic quenching accompanied by either static quenching or a transient component in dynamic quenching can result in the quadratic dependence of $[O_2]$. However, the quadratic form from equation (2) or (5) would result in an upperward curvature, because K_2 is positive. On the other hand, the experimental results show a downward curvature (Fig. 5). Thus, the latter seems to be more reasonable, taking the heterogeneous of these sensing systems into consideration. The quenching behavior of photoluminescent molecules is affected by the local composition in which the molecule is situated. Especially in heterogeneous systems, it is believed that there are inhomogeneities in the dye environment, i.e., two or more sites with different quenching constants are occupied by [Tb(acac)$_3$(phen)]: oxygen-easy accessible and oxygen-difficult accessible sites.[24,25] Therefore, in the case of a condensed system, such as a polymer film, the Stern–Volmer plot deviates from linearity because of the different relative contributions which originate from different quenching sites. Hence, the dependence of I_0/I on the oxygen concentration differs from Eq. 1,

$$I_0/I = [\Sigma(f_n/(1 + K_{SVn}[O_2]))]^{-1}, \quad (6)$$

where, the f_n is the fractional contributions to the oxygen-accessible site or oxygen-difficult accessible site. K_{SVn} is the quenching constant for each accessible site. In all monitored wavelengths, the best-fit curves were obtained when n was equal to 2, supported by the correlation factor, r^2, estimated to be 0.988 for 480 nm, 0.993 for 546 nm, 0.997 for 590 nm and 0.993 for 620 nm by least-squares method. In Fig. 5, the solid lines are the best fit using the above equation ($n = 2$). A [Tb(acac)$_3$(phen)] film sensor was calibrated by the modified Stern–Volmer equation (Eq. 6). Thus, there are two oxygen-accessible sites for the [Tb(acac)$_3$(phen)] film: one is an oxygen-accessible site ($K_{SV1} = 0.12\%^{-1}$($f_1 = 0.67$) for 480 nm, $K_{SV1} = 0.16\%^{-1}$($f_1 = 0.66$) for 546 nm, $K_{SV1} = 0.15\%^{-1}$($f_1 = 0.66$) for 590 nm, and $K_{SV1} = 0.16\%^{-1}$($f_1 = 0.66$) for 620 nm); and the other is an oxygen-difficult accessible site ($K_{SV2} = 0.0016\%^{-1}$($f_2 = 0.33$) for 480 nm, $K_{SV2} = 0.0016\%^{-1}$($f_2 = 0.34$) for 546 nm, $K_{SV2} = 0.0016\%^{-1}$($f_2 = 0.34$) for 590 nm, and $K_{SV2} = 0.0016\%^{-1}$($f_2 = 0.34$) for 620 nm).

Assuming that there are k-accessible (and n-k non-accessible) molecules with the same K_{SV}, Eq. 6 can be expressed as

$$I_0/(I_0 - I) = 1/(f K_{SV}[O_2]) + 1/f, \quad (7)$$

where, $f = \Sigma f_i$. This is the maximum mole fraction of dye molecules that are accessible to oxygen. If only a single class of dye molecules with the same accessibility to oxygen is present, $1/f$ in Eq. 7 should be 1. Figure 6 shows a modified Stern–Volmer plot for the [Tb(acac)$_3$(phen)] film plotted using Eq. 7. $I_0/(I_0 - I)$ against $1/[O_2]$ showed good linearity, which was enhanced compared with a plot of I_0/I *against* $[O_2]$. In order to obtain the f value, the regression line is extrapolated to $1/[O_2] = 0$. The values of f are 0.60 for 480 nm, 0.63 for 546 nm, 0.61 for 590 nm and 0.61 for 620 nm. The value of f indicates

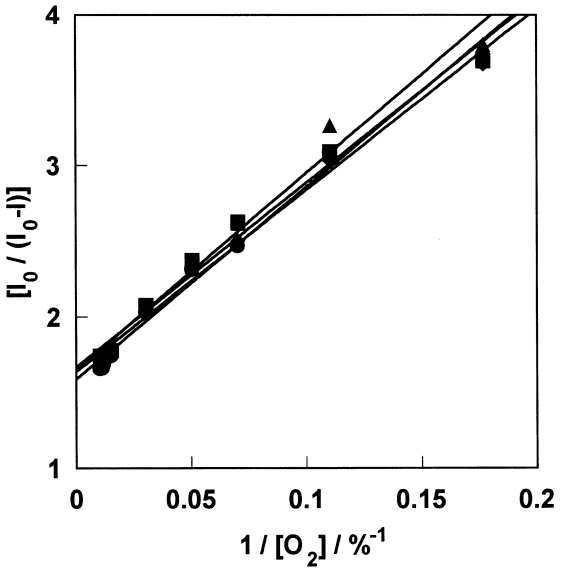

Fig. 6. The modified Stern–Volmer plot for [Tb(acac)$_3$(phen)] film using Eq. 7. Emission wavelength: (■) 490, (●) 546, (◆) 590 and (▲) 620 nm.

the oxygen quenching mole fraction of the [Tb(acac)$_3$(phen)] molecule, and $f = 1$ means that all excited [Tb(acac)$_3$(phen)] molecules are quenched equally by oxygen. Form the f values, the K_{SV} values $0.13\%^{-1}$ for 480 nm, $0.15\%^{-1}$ for 546 nm, $0.14\%^{-1}$ for 590 nm, and $0.13\%^{-1}$ for 620 nm, respectively. The K_{SV} and f values obtained from Eq. 7 were almost the same as the K_{SV1} and f_1 obtained from Eq. 6. Thus K_{SV1} was attributed to the luminescence quenching of [Tb(acac)$_3$(phen)] by oxygen. At all of the monitored wavelengths, K_{SV2} has a very low value, and a small contribution compared with K_{SV1}. Because the diffusion rate of oxygen is rapid in the film, the luminescence of [Tb(acac)$_3$(phen)] is fully quenched by oxygen. Thus, the oxygen-difficult accessible site is attributed to the static quenching site in the film (emission from background scattering, etc).

Figure 7 shows an operational stability test conducted by reading the luminescence intensity signal while oxygenated and deoxygenated gases were switched for 200 s. The response times are defined by the 95% response and recovery times, exhibited by the sensors when they were exposed to an alternating atmosphere of oxygen and argon, respectively. The response times of the [Tb(acac)$_3$(phen)] film were 7.3 s for switching from argon to oxygen, and 70 s for switching from oxygen to argon. Especially, the response time for switching from oxygen to argon was slow, compared with the response times of other optical oxygen sensors ($<$ 50 s). This result shows that the oxygen elimination was slow because of the strong interaction between [[Tb(acac)$_3$(phen)] and oxygen. The signal changes were fully reversible, and hysterisis was not observed during the measurements.

The dynamic response of the [Tb(acac)$_3$(phen)] film under various oxygen concentrations is shown in Fig. 8. This test was repeated and the signal changes were monitored when randomly increasing and decreasing the oxygen concentrations change. Evidently, the signal changes were fully reversible, and measurement hysterisis was not observed. An important

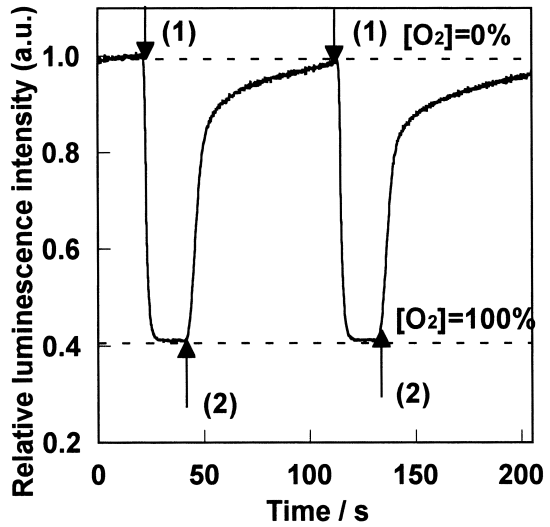

Fig. 7. Response time and relative intensity change for [Tb(acac)$_3$(phen)] film on switching between 100% argon (1) and 100% oxygen (2) for 200 s. Excitation and emission wavelengths were 268 and 546 nm, respectively.

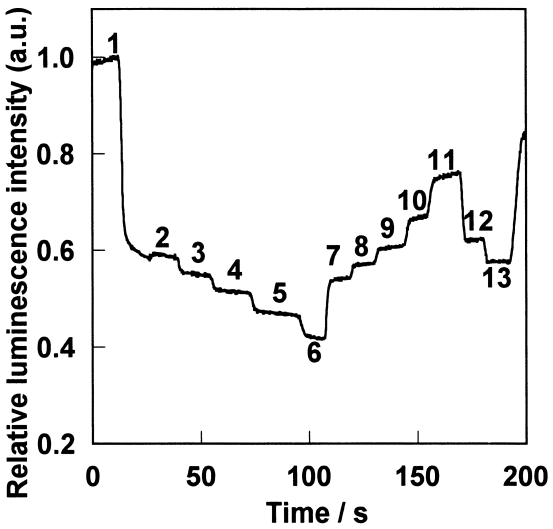

Fig. 8. Dynamic response of [Tb(acac)$_3$(phen)] film when oxygen concentrations were changed randomly. (1) 0; (2) 13.4; (3) 17.1; (4) 22.3; (5) 33.0; (6) 52.0; (7) 18.7; (8) 14.5; (9) 11.6; (10) 8.00; (11) 4.25; (12) 10.6; (13) 14.5% oxygen. Excitation and emission wavelengths were 268 and 546 nm, respectively.

factor for applying of the [Tb(acac)$_3$(phen)] film as an optical oxygen-sensing material is its photostability. To characterize the photostability of the [Tb(acac)$_3$(phen)] film, the reflectance spectrum of the film was measured after continuous irradiation using a 150 W tungsten lamp on the film for 24 h. No spectrum change was observed, indicating that the [Tb(acac)$_3$-(phen)] film is stable against irradiation.

Conclusion

A new photoluminescent oxygen sensor based on the luminescence intensities of tris(acethylacetonato)(1,10-phenanthroline)terbium(III) complex ([Tb(acac)$_3$(phen)]) adsorption film onto alumina plate was developed. The luminescence intensity of the [Tb(acac)$_3$(phen)] film decreased with increasing the oxygen concentration. The [Tb(acac)$_3$(phen)] film sensor was calibrated by the modified Stern–Volmer equation.

This work is partially supported by "Molecular Sensors for Aero-Thermodynamic Research (MOSAIC)," the Special Coordination Funds from the Ministry of Education, Culture, Sports, Science and Technology.

References

1 C. Prininger, I. Klimant, and O. S. Wolfbeis, *Anal. Chem.*, **66**,1841 (1994).
2 R. C. Martin, S. F. Malin, D. J. Bartnil, A. M. Schilling, and S. C. Furlong, *Proc. SPIE.*, **2131**, 426 (1994).
3 M. J. Atkinson, F. I. M. Thomas, N. Larson, E. Terrill, K. Morita, and C. C. Lium, *Deep-Sea Res. I.*, **42**, 761 (1995).
4 D. A. Skoog , D. M. West, and F. J. Holler, "Fundamentals of Analytical Chemistry," Saunders, Philadelphia (1988), p. 344.
5 L. C. Clark, *Trans. Am. Artif. Intern. Organs.*, **2**, 41 (1956).
6 T. M. Freeman and W. R. Seitz, *Anal. Chem.*, **53**, 98 (1981).
7 H. D. Hendricks, U.S. Patent 3709663 (1973).
8 H. W. Kroneis and H. J. Marsoner, *Sens. Actuators*, **4**, 587 (1983).
9 J. I. Peterson, R. V. Fitzgerald, and D. K. Buckhold, *Anal. Chem.*, **56**, 62 (1984).
10 S. K. Lee and I. Okura, *Anal. Chim. Acta*, **342**, 181 (1997).
11 E. R. Carraway, J. N. Demas, B. A. DeGraff, and J. R. Bacon, *Anal. Chem.*, **63**, 332 (1991).
12 X. M. Li, F. C. Ruan, and K. Y. Wong, *Analyst*, **118**, 289 (1993).
13 L. Huihui, I. Satoshi, K. Machida, and G. Adachi, *Chem Mater*, **11**, 3171 (1999).
14 J. Tetsuro Jin, I. Satoshi, S. Tsutsumi, K. Machida, and G. Adachi, *J. Non-Crystal Solids*, **223**, 123 (1998).
15 M. Iwamuro, T. Adachi, Y. Wada, T. Kitamura, and S. Yanagida, *Chem. Lett.*, **1999**, 539.
16 Y. Hasegawa, K. Sogabe, Y. Wada, T. Kitamura, N. Nakashima, and S. Yanagida, *Chem. Lett.*, **1999**, 35.
17 Y. Kawamura, Y. Wada, M. Iwamuro, T. Kitamura and S. Yanagida, *Chem. Lett.*, **2000**, 280.
18 N. E. Topp, "Chemistry of the Rare-earth Elements," Elesvier, Amsterdam (1965).
19 J. C. G. Bunzli and G. R. Choppin, "Lanthanide Probes in Life, Chemical and Earth Sciences," Elesvier, Amsterdam (1989).
20 K. M. Vallarino, "Handbook on the Physics and Chemistry of Rare Earths," Elesvier, Amsterdam (1991).
21 G. F. de Sá, O. L. Malta, C. de Mello Donegá, A. M. Simas, R. L. Longo, P. A. Santa-Cruz, and Jr. da Silva, *Coord. Chem. Rev.*, **196**, 165 (2000).
22 G. Vicentini, L. B. Zinner, J. Zukerman-Schpector, and K. Zinner, *Coord. Chem. Rev.*, **196**, 353 (2000).
23 Y. Amao, K. Asai, T. Miyashita, and I. Okura, *Chem. Lett.*, **1999**, 1031.
24 Y. Amao, K. Asai, and I. Okura, *Anal. Commun.*, **136**, 179 (1999).
25 J. N. Demas, B. A. DeGraff, and W. Xu, *Anal. Chem.*, **67**, 1377 (1995).